Received: 15 July 2018 | Revised: 16 March 2019 | Accepted: 22 April 2019 | Published on: 20 May 2019

DOI: 10.1002/joc.6112

RESEARCH ARTICLE

International Journal of Climatology RMetS

An evaluation of East Asian summer monsoon forecast with the North American Multimodel Ensemble hindcast data

Huiwen Nie[1] | **Yan Guo**[1,2]

[1]State Key Laboratory of Earth Surface Processes and Resource Ecology, Beijing Normal University, Beijing, China

[2]Zhuhai Joint Innovative Center for Climate-Environment-Ecosystem, Future Earth Research Institute, Beijing Normal University, Zhuhai, China

Correspondence
Yan Guo, State Key Laboratory of Earth Surface Processes and Resource Ecology, Beijing Normal University, Beijing 100875, China.
Email: guoyan@bnu.edu.cn

Funding information
NSFC Project, Grant/Award Number: 41305053; the National Programme on Global Change and Air-Sea Interaction, Grant/Award Number: GASI-IPOVAI-03

Abstract

The abilities of three models (Climate Forecast System version 2 [CFSv2], Canadian Coupled Climate Model version 3 [CanCM3] and Canadian Coupled Climate Model version 4 [CanCM4]) in the North American Multimodel Ensemble for the East Asian summer monsoon (EASM) forecast were evaluated with their 29-year hindcast data (1982–2010). Many EASM features including monsoon precipitation centres, large-scale monsoon circulations and monsoon onset and retreat are generally captured by the three models and their ensemble mean, and the multimodel ensemble has the best performance. Since the East Asian domain includes the tropical western North Pacific summer monsoon (WNPSM) and the subtropical continent monsoon, two well-known monsoon indices, the WNPSM index (WNPSMI) and EASM index (EASMI), and their associated low-level winds and precipitation anomalies are well forecasted by the models. However, the forecast performance generally decreases as the leads increase, and the performance of EASMI is not as good as that of WNPSMI. CFSv2 forecasts well at leads up to 6 months whereas the skill of CanCM3 (CanCM4) decreases rapidly when the lead increases to 2 months (3 months). The failure of CanCM3 is mainly attributed to the poor forecast of the relationship of EASMI with the El Niño-Southern Oscillation and Northern Indian Ocean-western North Pacific (WNP) sea surface temperature anomaly. However, the causes of the poor forecast of CanCM4 for EASMI require further investigation. Sources of the forecast error (FE), which is the difference between model and observation for monsoon precipitation, are more significant than those of the predictability error (PE), which originates from the initial condition error, indicating that model deficiency plays a dominant role in limiting the EASM precipitation forecast. However, the PE cannot be neglected over the tropical western Pacific in CFSv2, over the WNP in CanCM3 and over the Tibetan Plateau in CanCM4. As the lead time increases, the FE does not remarkably change whereas the PE decreases significantly.

KEYWORDS

East Asian summer monsoon, forecast error, North American Multimodel Ensemble, precipitation, predictability error

1 | INTRODUCTION

The East Asian summer monsoon (EASM), which is characterized by the heaviest seasonal precipitation, affects approximately one third of the world's population. EASM precipitation is crucial for agriculture, water resources, energy and transportation. Due to its pronounced interannual and decadal variability, the EASM can cause serious natural disasters such as extreme floods and severe droughts (Ding, 1991; Huang *et al*., 1998; Huang and Zhou, 2002; Huang, 2014). Therefore, it is significant to understand the physical mechanism of the EASM variation and provide reliable forecasts of the EASM.

The predictability on seasonal to interannual time scales mainly stems from the slowing varying boundary conditions. Sea surface temperature (SST) anomalies associated with basin-wide events such as the El Niño-Southern Oscillation (ENSO), North Atlantic SST triple, Indian Ocean dipole (IOD), Indo-Pacific warm pool and North Pacific Ocean dipole (IPOD) are primary predictability sources for the EASM seasonal forecast (Wang *et al*., 2000; Yuan *et al*., 2008; Wu *et al*., 2009; Zheng *et al*., 2014). Due to advances in the understanding of air–sea interaction and computing capability, one-tier systems using fully coupled climate models are routinely used for seasonal forecast at several weather and climate centres worldwide. The European Centre for Medium-Range Weather Forecasts System 4 (ECMWF4), Climate Forecast System version 2 (CFSv2), Canadian Centre for Climate Modelling and Analysis (CCCma) Coupled Climate Model 4 (CanCM4) and Global Seasonal forecast system version 5 (GloSea5) are the latest operational seasonal forecast systems in the ECMWF, National Center for Environment Prediction (NCEP), CCCma and Met Office, respectively (Molteni *et al*., 2011; Merryfield *et al*., 2013; Saha *et al*., 2014; MacLachlan *et al*., 2015). A variety of studies have evaluated these forecast systems. Kim *et al*. (2012) compared the forecast skill of CFSv2 and ECMWF4 for the EASM and found that both models capture the variability of large-scale monsoon circulation but have poor performance in reproducing monsoon precipitation. Zuo *et al*. (2013) showed the good performance of CFSv2 in forecasting the monsoon precipitation patterns associated with the ENSO due to its good forecast skill for ENSO. GloSea5 is useful to forecast the western North Pacific subtropical high (WNPSH) that largely determines the summer precipitation over East Asia (MacLachlan *et al*., 2015). Li *et al*. (2016) also demonstrated that GloSea5 is good at forecasting the summer rainfall over the Yangtze river valley, and suggested that the predictability corresponds to skilful prediction of rainfall in the deep tropics and around the Maritime Continent.

Multimodel ensemble (MME) is a more effective approach to reduce forecast bias (Krishnamurti *et al*., 1999; Krishnamurti *et al*., 2000). After the European Multimodel Ensemble System for Seasonal to Interannual Prediction project DEMERTER (2000) and ENSEMBLES (2004), the United States launched the North American Multimodel Ensemble (NMME) forecast project (Kirtman *et al*., 2014), phase I of which is the seasonal-to-interannual forecast and phase II is developing the intraseasonal forecast. The NMME consists of nine coupled forecast systems from several modelling centres in North America and provides real-time forecasts since August 2011. In addition to real-time forecasts, each model provides hindcasts covering the last three decades. CFSv2, CanCM3 and CanCM4 are three partner models with complete hindcast data available. CFSv2 is an improved version of CFSv1 in all aspects including the model components, data assimilation system and ensemble configuration. Generally, it has moderate forecast skill in global monsoon precipitation and shows higher skill than CFSv1 (Shi *et al*., 2011; Yuan *et al*., 2011; Saha *et al*., 2016). However, CFSv2 has some biases in the Asian summer monsoon precipitation forecast (Jiang *et al*., 2013). Compared with CFSv2, whose fidelity has been widely evaluated, few studies have evaluated CanCM3 and CanCM4 in forecasting the EASM. In this work, we focus on the above three models and their MME, and evaluate their performance for the EASM forecast. This is a prerequisite for selecting superior models to enhance the forecast skill for the EASM.

In this study, we focus on three issues of the EASM forecast. First, the 0-month lead forecasts are evaluated for the climatological EASM circulations and precipitation, the annual cycle of precipitation, and the year-to-year variation of the EASM. Second, the forecast accuracy for EASM indices at different leads are examined and the possible reasons for incorrect forecasts are studied. Finally, sources of the forecast error for EASM precipitation are analysed. The remainder of this paper is organized as follows. Section 2 introduces the model hindcast data and the observational data for verification. The evaluation of the 0-month lead forecast is described in Section 3. Section 4 shows the forecast skills at different leads and analysis of possible causes of the forecast failure. Section 5 provides an analysis of the sources of the forecast error for EASM precipitation. A brief summary and discussion are given in Section 6.

2 | DATA

Three models in the NMME are used in this study, CFSv2, CanCM3 and CanCM4. CFSv2 is the second version of the fully coupled operational forecast system at the NCEP. It consists of the GFS at T126 resolution, MOM4 at $0.25^\circ \times 0.25^\circ$ grid coupled with a four-layer Noah land

surface model and a two-layer interactive global sea ice model. Its 9-month run initiates every 5 days with 4 cycles (0000, 0600, 1,200 and 1800 UTC) on those days. To reflect the uncertainty of the initial conditions, a 24-member ensemble is formed for each month with initial dates after the seventh of the previous month (Saha *et al*., 2014). CanCM3 (CanCM4) uses the CCCma's third- (fourth-) generation atmospheric general circulation model CanAM3, T63/L31 (CanAM4, T63/L35) and CCCma's ocean model CanOM4 (1.41° × 0.94°/L40). Each hindcast is initiated every month and integrates 12 months, and has 10 ensemble members originated from different initial conditions (Merryfield *et al*., 2013). In this study, the model assessment period is 1982–2010. For each model, only the multimember ensemble mean is employed. For the June–July–August (JJA) mean EASM, the 0-month lead forecast is the forecast initiated in the beginning of June. In addition to 0-month lead forecast, forecasts at different leads were also evaluated.

Observational data used for verification include the Global Precipitation Climatology Project (GPCP) precipitation dataset version 2.3 on a 2.5° × 2.5° grid (Adler *et al*., 2018), the ERA-Interim reanalysis dataset on a 1° × 1° grid (Berrisford *et al*., 2009) and the NOAA Extended Reconstructed Sea Surface Temperature (ERSST) dataset on a 2° × 2° grid (Huang *et al*., 2015). For comparison, all the model hindcast and observational data were interpolated into a common 1° × 1° grid with the bilinear interpolation method.

3 | 0-MONTH LEAD FORECAST

In this section, the 0-month lead forecasts of the EASM of the three models (CFSv2, CanCM3 and CanCM4) and their ensemble mean are evaluated in terms of the climatological features and year-to-year variation.

3.1 | Climatological features

Figure 1 shows the observed JJA mean precipitation and winds at 850 and 200 hPa and the forecast biases from the individual models and their ensemble mean. At the low level, it is characterized by a monsoon trough over the South China Sea (SCS), southwesterly over the western North Pacific (WNP) and the WNPSH. Associated with this circulation, several heavy precipitation centres appear over the SCS and WNP (Figure 1a). These major features are basically reproduced by the three models, with some biases. CFSv2 shows an abnormally weak monsoon trough over the SCS and a weak WNPSH. It overestimates the precipitation over the south SCS and underestimates the precipitation around Korea and the Yangtze-Huaihe River basin in China (Figure 1b). CanCM3 shows a northward-shifted WNPSH, resulting in a strong dry bias over Southern China and south

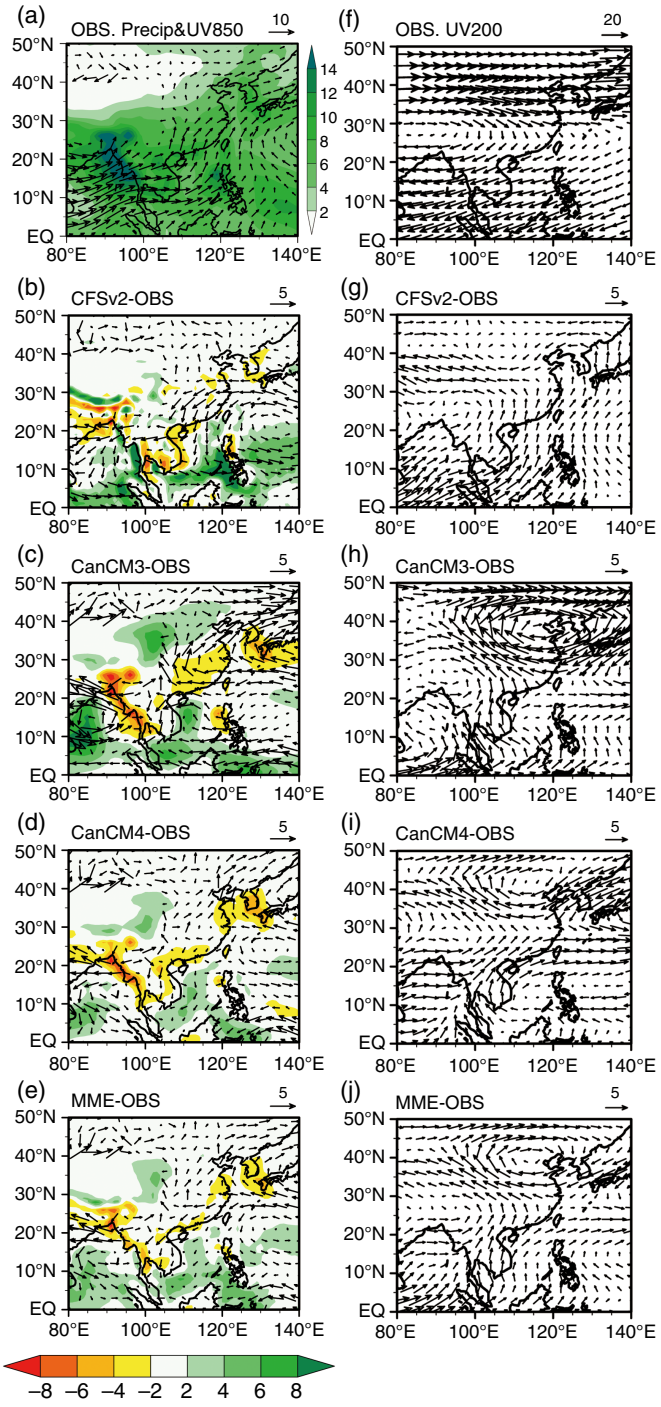

FIGURE 1 The climatology (1982–2010) of (a) JJA precipitation (mm day^{-1}, shading) and 850 hPa winds (m s^{-1}, vectors) from observations, and the corresponding forecast bias (0-month lead) for (b) CFSv2, (c) CanCM3, (d) CanCM4 and (e) the three-model ensemble mean. (f)–(j) as in (a)–(e) but for 200 hPa winds

of Japan. Wet biases are observed over the SCS and northwestern China (Figure 1c). CanCM4 generally exhibits the same bias pattern as CanCM3 with obviously smaller magnitude (Figure 1d). The ensemble mean generally appears to be better than the individual models, although it has the bias

of a northward-shifted WNPSH with suppressed precipitation there (Figure 1e). At the upper level, it is characterized with a Tibetan anticyclone with a westerly jet over its north side and an easterly jet over its south side (Figure 1f). The individual models and their ensemble mean obviously underestimate the Tibetan anticyclone. CanCM3 and CanCM4 also show a bias of anticyclone over northeast China (Figure 1h–i). The biases from CFSv2 and MME are relatively small.

In addition to the summer mean precipitation, the intraseasonal variation of precipitation was examined. Figure 2 shows the time-latitude cross sections of precipitation averaged over 110°–140°E from observation, the individual models and their ensemble mean. In the observation, the maximum precipitation centre is located at approximately 5°N from January to April and, after April, abruptly jumps northward to approximately 15°N, which corresponds to the earliest monsoon onset over the SCS (Wang and LinHo, 2002; Wang *et al*., 2004). After the SCS monsoon onset, one maximum precipitation centre advances northward to 30°N in June and continues to move northward in July at a relatively quick pace and abruptly retreats southward in September, which corresponds to the East Asian rainfall season (Ding and Chan, 2005); the other maximum precipitation centre remains at approximately 15°N and then gradually retreats, which corresponds to the WNP summer monsoon (WNPSM) rainfall (Wu and Wang, 2000). In addition, a premonsoon rainfall belt, mainly due to the frontal systems, appears at approximately 25°N–30°N (Wan and Wu, 2007) (Figure 2a). The individual models generally capture the month-to-month evolution of EASM precipitation but underestimate the first maximum precipitation centre (Figure 2b–d). CFSv2 can reproduce monsoon onset and retreat well, but the WNPSM rainfall belt is southward-shifted (Figure 2b). Both CanCM3 and CanCM4 show earlier monsoon onset and retreat (Figure 2c,d). The MME

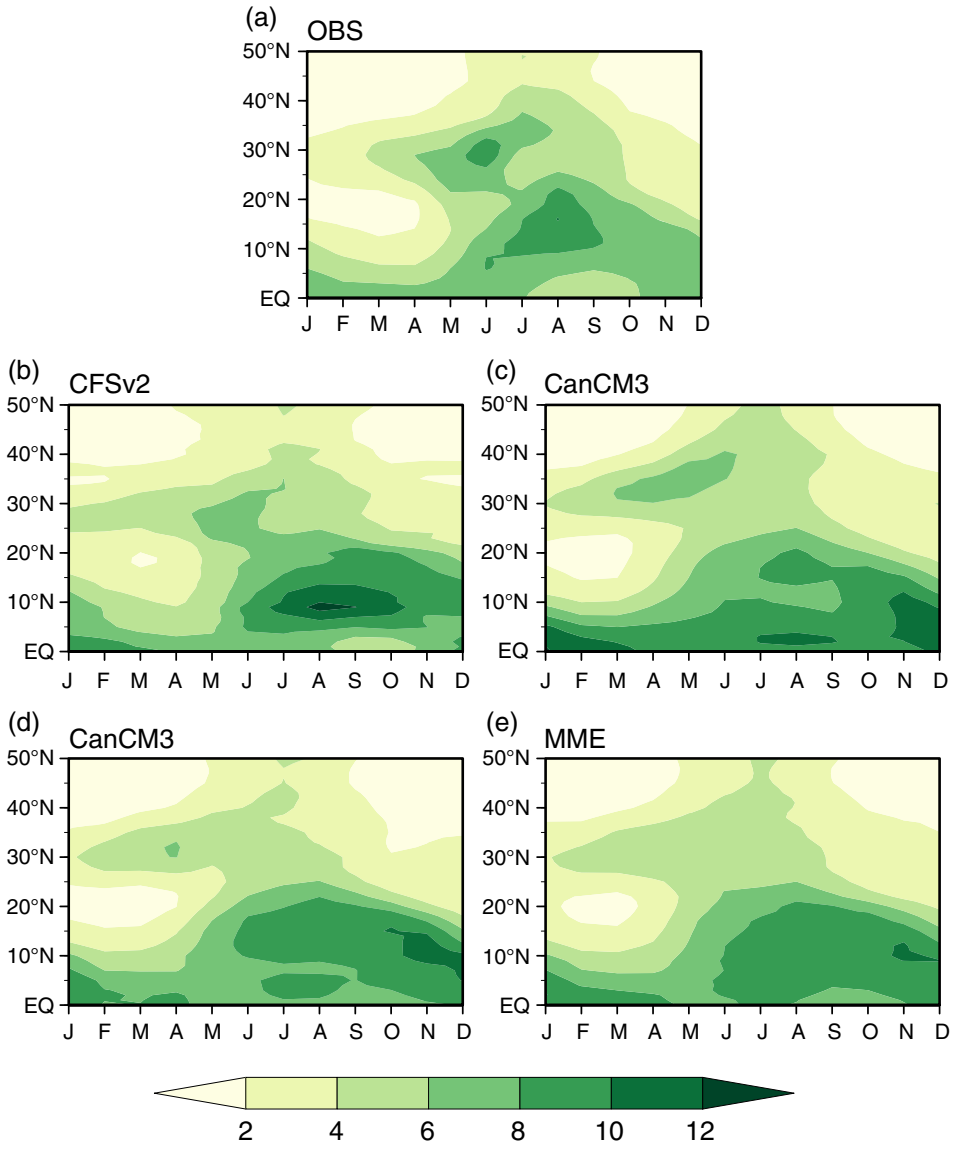

FIGURE 2 Time-latitude sections of climatological (1982–2010) precipitation (mm day^{-1}) averaged over 110°–140°E from (a) observations, 0-month lead forecast based on (b) CFSv2, (c) CanCM3, (d) CanCM4 and (e) the three-model ensemble mean

does not reproduce the evolution of EASM precipitation well (Figure 2e).

3.2 | Year-to-year variation

In addition to the distribution of climatological monsoon circulation and precipitation, the year-to-year variation was also evaluated. Figure 3 shows the spatial distributions of the temporal correlation coefficient (TCC) between observations and the forecasted JJA precipitation, 850 hPa zonal and meridional winds from CFSv2, CanCM3, CanCM4 and their ensemble mean. It seems that precipitation is very difficult to forecast, with insignificant TCCs in most East Asian regions except the tropics (Figure 3a–d). The low-level monsoon circulation is better forecasted than precipitation, showing superiority over southeast China and the WNP

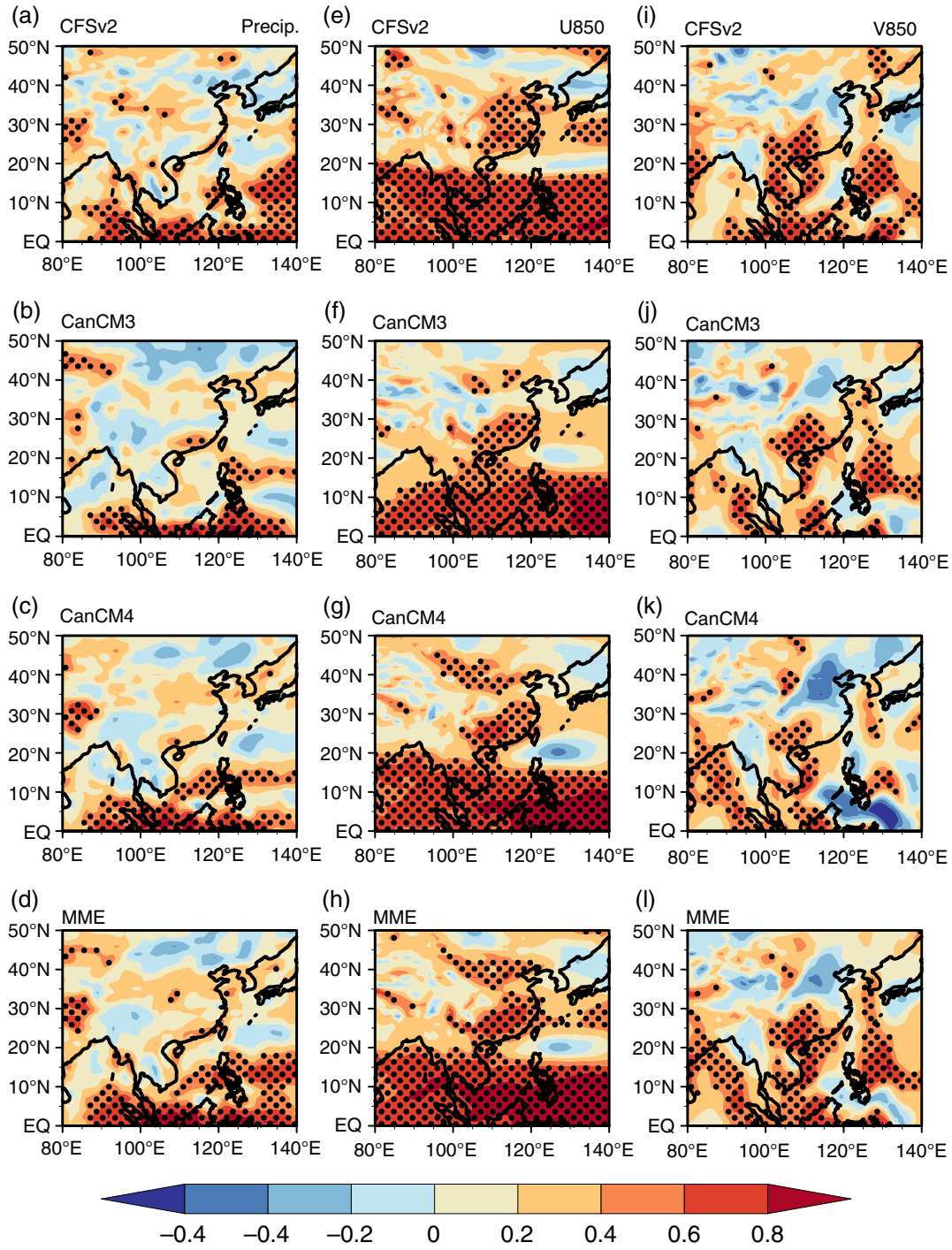

FIGURE 3 The temporal correlation coefficients (1982–2010) of JJA precipitation (left), zonal (middle) and meridional winds (right) at 850 hPa between the observations and forecast (0-month lead) of CFSv2, CanCM3, CanCM4 and the three-model ensemble mean. The black dots depict the 0.05 significance level

(Figure 3e–l). In addition, the forecast skill of CFSv2 for precipitation and meridional winds is better than that of CanCM3 and CanCM4, and the MME showed the best zonal winds forecast performance.

Monsoon indices are defined to describe the year-to-year variation of EASM strength. Since the East Asian domain includes the tropical WNPSM and the subtropical continent monsoon, two well-known monsoon indices defined in previous studies are employed here. One is the WNPSM index (WNPSMI), defined (Wang and Fan, 1999) as a normalized difference of the 850 hPa zonal wind between 5°–15°N, 100°–130°E and 20°–30°N, 110°–140°E. The WNPSMI largely reflects the features in low latitudes and is well-studied (Wang *et al*., 2001; Cherchi and Navarra, 2002; Sooraj *et al*., 2014). The other is the EASM index (EASMI), defined (Zhao *et al*., 2015) as a normalized tripole of 200 hPa zonal wind anomaly, that is, u (2.5°–10°N, 105°–140°E) − u (17.5°–22.5°N, 105°–140°E) + u (30°–37.5°N, 105°–140°E). The EASMI reflects the circulation feature over WNP and the related features over the mid-latitudes and tropics. The fidelity to reproduce above two monsoon indices and their associated

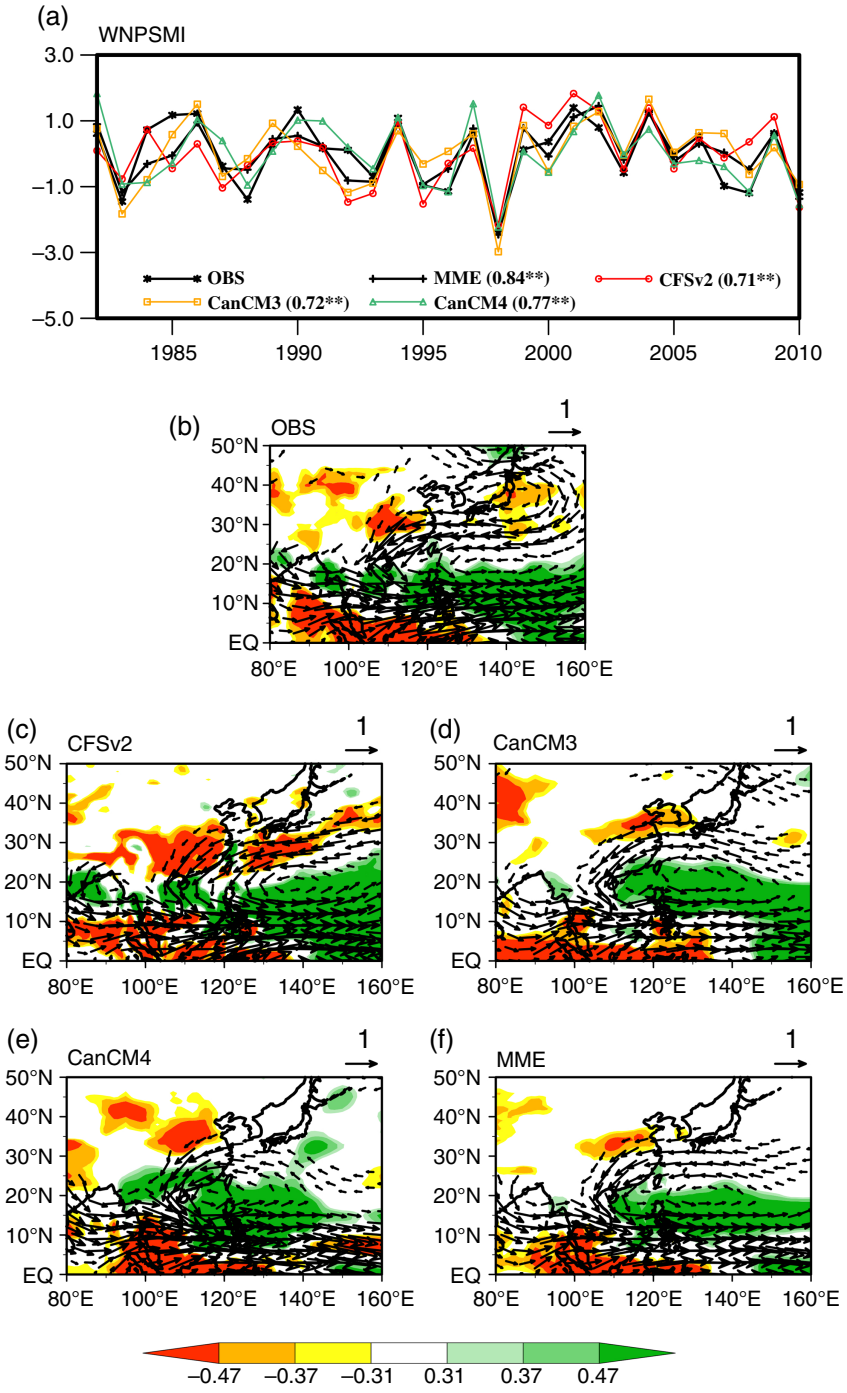

FIGURE 4 (a) The evolution (1982–2010) of the WNPSMI with the ERA-interim, three-model ensemble mean, CFSv2, CanCM3 and CanCM4. The distribution of correlation coefficients of the WNPSMI with JJA precipitation (shading) and regression coefficients of WNPSMI for 850 hPa winds (vector) from (b) observations, (c) CFSv2, (d) CanCM3, (e) CanCM4 and (f) the three-model ensemble mean. Precipitation and wind vectors below the 0.1 confidence level are omitted

circulation and precipitation anomaly patterns are evaluated in the following section.

Figure 4 shows the year-to-year variation of the WNPSMI and its associated patterns of JJA precipitation and 850 hPa wind anomalies from observations, the individual models and their ensemble mean. All models reasonably reproduce the year-to-year variation of WNPSMI, with TCCs of 0.71, 0.72 and 0.77 for CFSv2, CanCM3 and CanCM4, respectively, exceeding the 0.01 significance level. The MME performs better than individual models and has the highest TCC of 0.84 (Figure 4a). Associated with the positive WNPSMI anomaly, an anomalous westerly appears over the tropical Indo-Pacific Ocean and an anomalous cyclone and anticyclone appear over the WNP and the Japan Sea. The WNPSMI has significant positive correlation with the precipitation over the WNP and negative correlation over the Meiyu-Changma-Baiu (Figure 4b). All models generally capture the associated pattern of low-level circulation and precipitation anomalies with the WNPSMI. However, the negative correlation of the WNPSMI with precipitation is overestimated over the Meiyu-Changma-Baiu in CFSv2 (Figure 4c). In CanCM3/CanCM4, the associated winds are

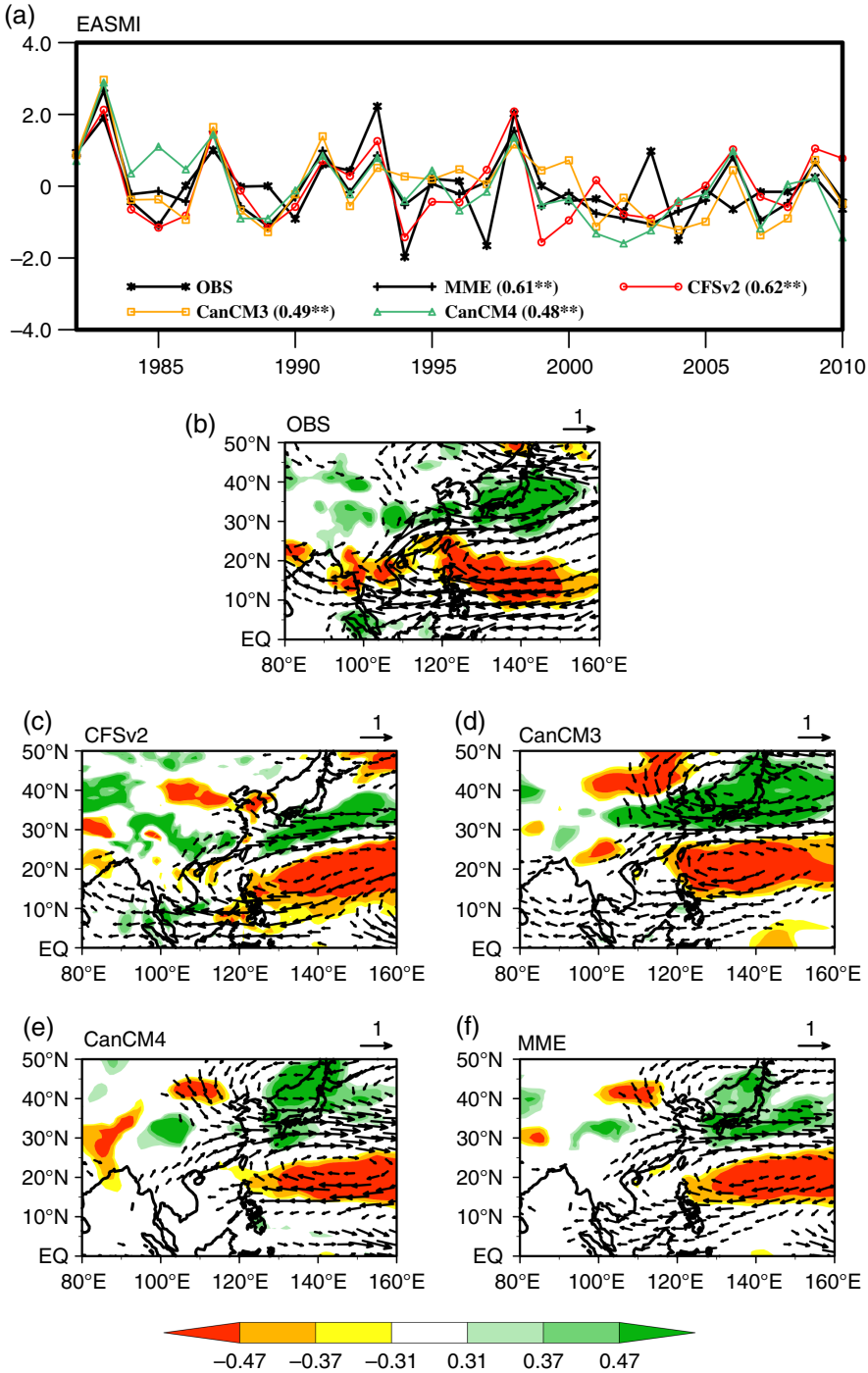

FIGURE 5 As in Figure 4 but for the EASMI

abnormally weak and the meridional distribution of the correlation between the WNPSMI and precipitation is shifted northward (Figure 4d–e). For the MME, the associated low-level winds and precipitation are also generally slightly weaker (Figure 4f).

Figure 5 shows the year-to-year variation of the EASMI and its associated patterns of precipitation and 850 hPa winds. Compared with the WNPSMI, the forecast skill for EASMI is slightly lower, with TCCs of 0.62, 0.49, 0.48 and 0.61 for CFSv2, CanCM3, CanCM4 and the MME, respectively, but still exceeding the 0.01 significance level. Associated with the positive EASMI anomaly, an anomalous easterly appears over the tropical Indo-Pacific Ocean and an anomalous cyclone and anticyclone appear over the WNP and the Japan Sea. The correlation of the EASMI with precipitation is significant positive over the Meiyu-Changma-Baiu and negative over the WNP. The models reproduce the major features in the observed patterns, with some biases in strength and displacement. CFSv2 shows an extremely weak cyclonic anomaly over the Japan Sea and a slightly southward-shifted meridional distribution of precipitation anomalies (Figure 5c). In CanCM3, the associated meridional distribution of the correlation is slightly northward-shifted (Figure 5d). In CanCM4 and the MME, the associated patterns are well captured, although the associations are mainly in the Pacific (Figure 5e,f).

The WNPSMI is better forecasted than the EASMI, which has been indicated in evaluations on other climate models (Lee *et al*., 2011; Park *et al*., 2018). This result is consistent with those shown in Figure 3 that higher TCCs appear both in 850 hPa zonal wind over the WNP and in precipitation over the Maritime Continent and east of the Philippines. Similarly, good forecasts over the WNP were also seen in ENSEMBLES models (Li *et al*., 2012).

4 | FORECAST SKILLS AT DIFFERENT LEADS

Figure 6 shows the forecast skills for the WNPSMI and EASMI at leads of 0 to 6 months based on CFSv2, CanCM3, CanCM4 and their ensemble mean. Despite a few fluctuations, the forecast skill generally decreases as the leads increase. For the WNPSMI, the models and their ensemble mean provide an acceptable forecast at leads up to 6 months (Figure 6a). In contrast, the forecast skill for EASMI is not as good as that of WNPSMI. Only CFSv2 shows an acceptable forecast at leads up to 6 months. The forecast skill of CanCM3 (CanCM4) decreases rapidly when the leads exceed 2 months (3 months), although the performance of CanCM4 at 5-month lead is acceptable (Figure 6b).

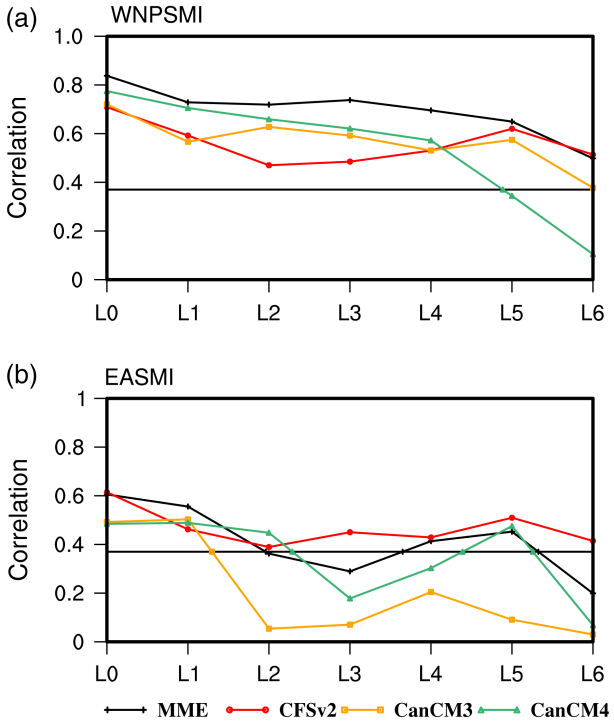

FIGURE 6 Correlation coefficients of the forecasted (a) WNPSMI and (b) EASMI and observations at different leads. The grey horizontal line for 0.37 indicates the 0.05 confidence level

What are the factors limiting the forecast skill of the EASMI at long leads? In the following, we analyse the possible causes. A variety of studies revealed that the ENSO has an important influence on the EASM in the decaying summer through an anomalous anticyclone over the WNP that is triggered by ENSO and maintained by ENSO-induced Indian Ocean (IO) warming (Zhang *et al*., 1996; Wang *et al*., 2000; Du *et al*., 2009; Xie *et al*., 2016). Figure 7 shows the spatial distribution of the TCCs of the EASMI with the monthly global SST from the preceding December to August in observation. Corresponding to the positive EASMI anomaly, two SST anomaly (SSTA) signals are notable. One is the El Nino-typed SSTA over 10°S–10°N, 80°–150°W from the preceding December to May and the other is the warming SSTA over the Northern IO and WNP (NIOWNP, 0°–20°N, 50°–130°E) from May to August. Accordingly, two SSTA indices are defined as the area-averaged SSTA to describe the above two signals, that is, ENSO and NIOWNP. Figure 8a shows the lead–lag correlation of the EASMI with the monthly ENSO and NIOWNP indices from the preceding December to the simultaneous December. The ENSO index has a significantly positive correlation with the EASMI from the preceding December to May, and the NIOWNP index has a significantly positive correlation from May to July. These results are consistent with the previous finding from Zhao *et al*. (2015).

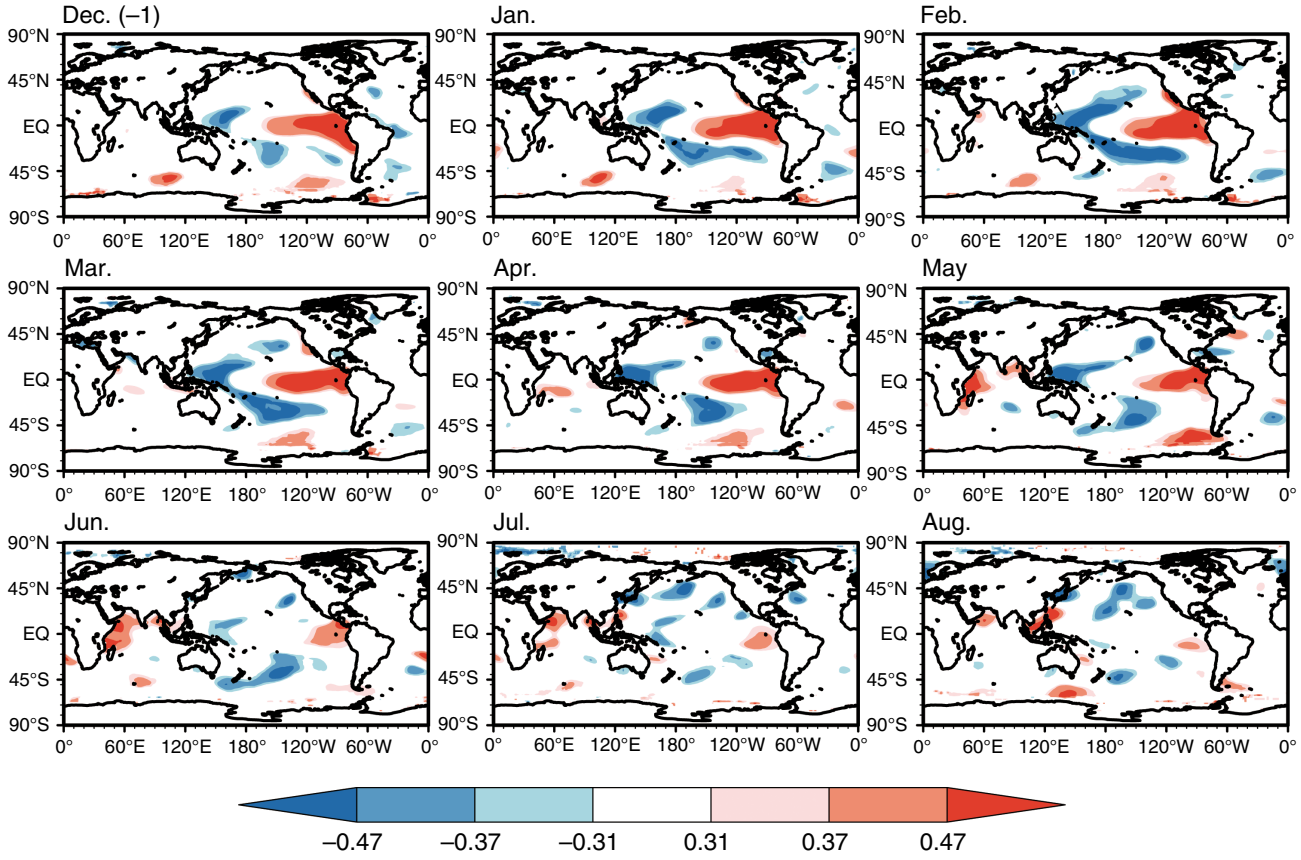

FIGURE 7 The correlation coefficients (1982–2010) of the monthly SST with the EASMI from the preceding Dec. to Aug. in observation. Correlation coefficients of 0.31, 0.37 and 0.47 correspond to the 0.1, 0.05 and 0.01 confidence levels, respectively

How well do CFSv2, CanCM3 and CanCM4 reproduce the observed relationship of the EASMI with the ENSO and NIOWNP indices? The cross-correlations of the EASMI with the ENSO and NIOWNP indices for all forecasts with start times from the preceding December to June (corresponding to the L6, L5, L4, L3, L2, L1 and L0 forecasts) and all integration months are shown in Figure 8b–g. For example, the first column from bottom to top in Figure 8b shows the TCCs of the EASMI and monthly ENSO index from the start time (preceding December) to the 10th integration month (September) for CFSv2. The area between the two diagonals in Figure 8b represents June to August. CFSv2 reasonably reproduced the relationships of EASM with both the ENSO and the NIOWNP SSTA in all lead forecasts (Figure 8b,c). CanCM3 failed to reproduce the relationship between the EASM and the ENSO from the preceding winter to April in three lead forecasts initiated in the preceding December, January and February, respectively (Figure 8d). Moreover, the relationship between the EASM and the NIOWNP SSTA from May to July is generally missed in CanCM3 forecasts except two forecasts initiated in May and June (Figure 8e). The failure of CanCM3 to capture the observed relationship of the EASM with the precursory ENSO and NIOWNP SSTA is responsible for its low skill in forecasting the EASMI at leads from 2 to 6 months (Figure 6b). Compared with CanCM3, CanCM4 can generally reproduce the observed relationships of the EASM with the ENSO and NIONWP SSTA, although the relationship with the NIONWP SSTA in May is missed in most forecasts (Figure 8g), which might affect its forecast skill for the EASMI. However, the failure of CanCM4 in forecasting the observed relationship of the ENSO and NIONWP SSTA does not exactly match its low skill in forecasting the EASMI at leads of 3, 4 and 6 months (Figure 6b), which suggests other causes may contribute to the forecast failure in CanCM4.

In addition to reproduction of the relationships between the EASM and precursors such as the ENSO and NIOWNP SSTA, the fidelities to forecast precursors were examined because they also affect a model's forecast skill for the EASMI. Figure 9 shows the forecast skill (measured by TCC) for the ENSO and NIOWNP indices from CFSv2, CanCM3 and CanCM4 for all forecasts with start times from the preceding December to June and all integration months. The figure shows that the models can forecast the above two precursors well.

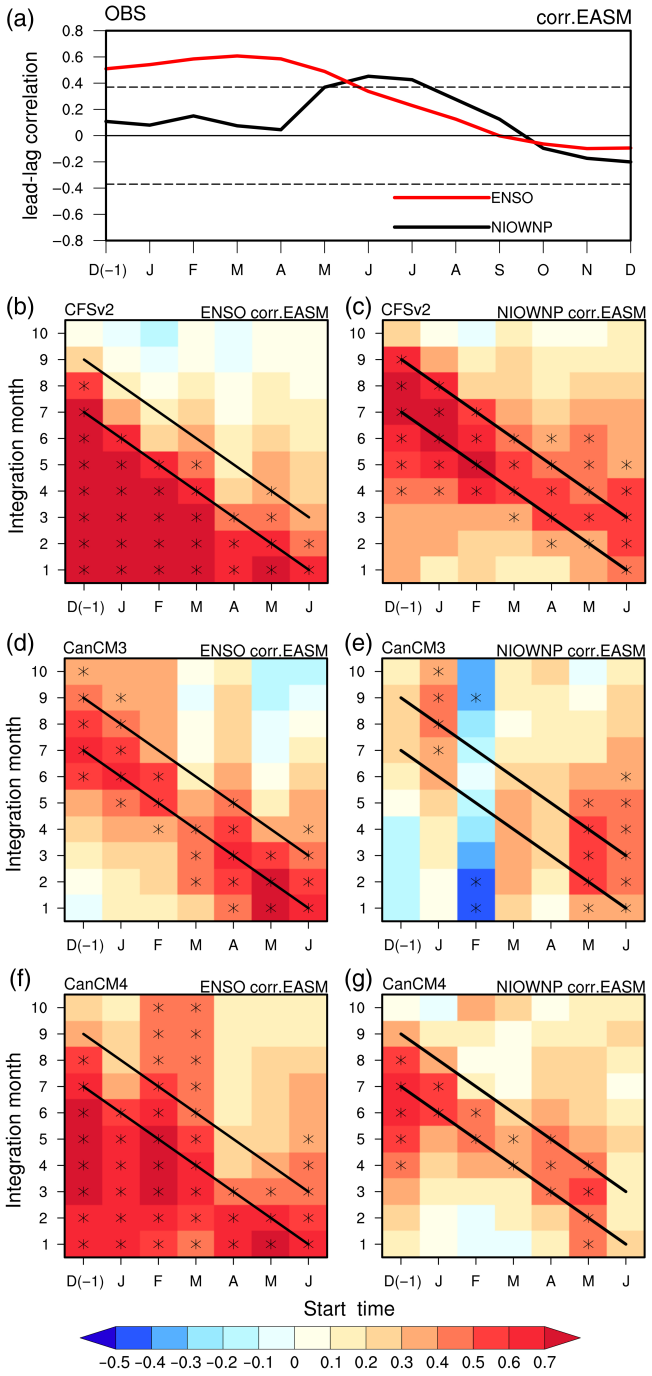

FIGURE 8 (a) Lead–lag correlation of the EASMI with the ENSO and NIOWNP indices from the preceding Dec. to Dec. Cross-correlation as a function of start time and integration month of the EASMI with the ENSO and NIOWNP indices of CFSv2 (top), CanCM3 (middle) and CanCM4 (bottom) forecasts. The area between the two slanting lines indicates the JJA season. The stars represent the 0.05 significance level

5 | FORECAST ERROR AND PREDICTABILITY ERROR OF EASM PRECIPITATION

After examining the models' forecast of monsoon indices, more quantitative analyses on the precipitation forecast error were conducted. The predictability of a model is featured by two types of errors. One is the initial condition error and the other is the model error arising from the imperfection of the model due to its parameterization schemes, resolution, and truncation (Pokhrel *et al.*, 2016). Forecast error (FE) refers to the difference between the model and observation, which represents the error due to all possible reasons such as model physics, dynamics, and initial conditions. Assuming the model is perfect, the predictability error (PE) largely originates from the initial condition error. Following the approach of Lee Drbohlav and Krishnamurthy (2010), the PE is defined as the difference between the model's two adjacent lead forecasts, 1 month apart (e.g., PE of L1 = L1 − L0). The difference is quantified by the root mean square error (RMSE). Therefore, the FE and PE in i-th year at j-th lead are

$$FE_j = \sqrt{\frac{\sum_{i=1}^{N-1}\left(X_{i,j} - O_i\right)^2}{N}}$$

$$PE_j = \sqrt{\frac{\sum_{i=1}^{N-1}\left(X_{i,j} - X_{i,j-1}\right)^2}{N}}$$

where $X_{i,j}$ is the forecast in the *i-th* year at the *j-th* lead of a sample of N years (1982–2010). O_i is the observation in the *i-th* year.

The FE and PE of the JJA mean precipitation in CFSv2, CanCM3 and CanCM4 with different leads were calculated and are shown in Figures 10–12. The FE is much larger than the PE in the forecasts with the same leads, indicating that model error rather than initial condition error is the dominant source of the precipitation forecast error. In addition, the PE generally decreases as the leads increase, which has been interpreted as the initial condition effect becoming trivial as the integration time increases (Charney and Shukla, 1981).

The locations of the FE and PE vary in the individual models. For CFSv2 (Figure 10), the maximum FE centres are mainly located over the Korea-Japan region, South China, the SCS, the Philippine Sea and the tropical WNP and the maximum PE centres are mainly concentrated over the SCS and the tropical WNP. The FE is much larger than the PE over the SCS, the Philippine Sea and the tropical WNP, which indicates that the model deficiency mainly causes the precipitation error in those areas. Conversely, the PE is considerable over the WNP, meaning that initial condition error primarily accounts for the FE there. Notably, although the PE usually decreases as the leads increase, the PE over the tropical western Pacific at L2 is almost the largest (Figure 10h). This is consistent with the result reported by Pokhrel *et al.* (2016), who speculated that it may be

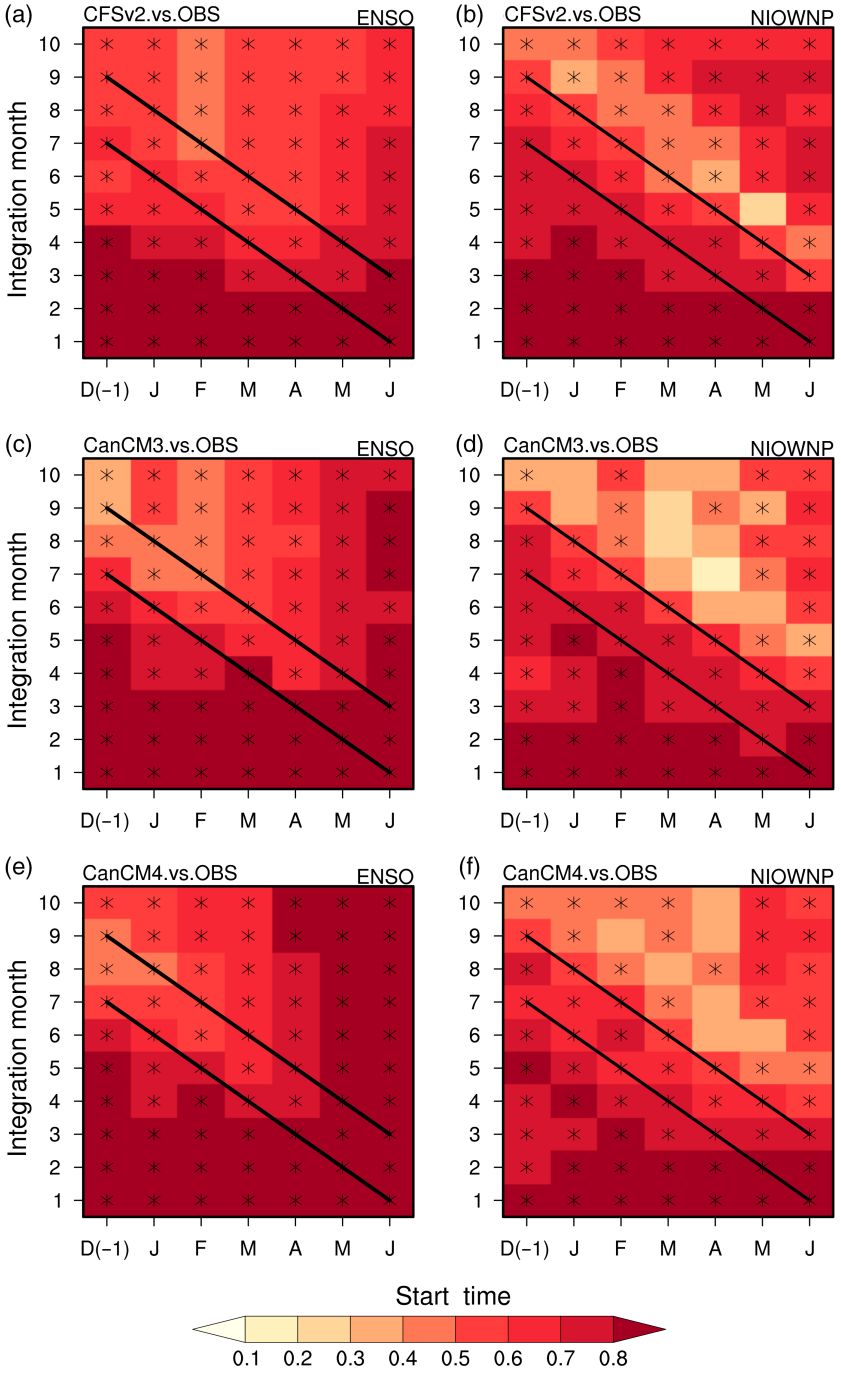

FIGURE 9 Correlation as a function of start time and integration month of the forecasts in CFSv2 (top), CanCM3 (middle) and CanCM4 (bottom) and observations for the ENSO and NIOWNP indices. The area between the two slanting lines indicates the JJA season. The stars represent the 0.05 significance level

associated with the spring predictability barrier (SPB) of the ENSO.

For CanCM3 (Figure 11), the FE is mainly located over central China, southwest Japan, Southern China and the SCS (Figure 11a–f). The PE, which wanes as the leads increase, is mainly distributed over central China, southwest Japan, and the WNP (Figure 11g–l). Comparing these two types of error, we speculate that the large FE over central China and the SCS is primarily caused by model deficiency.

Figure 12 shows the FE and PE for CanCM4. The FE centres are mainly located over western China, the Korea-Japan region, Southern China and the SCS (Figure 12a–f). The PE errors are smaller and are mainly distributed over western China, southwest Japan and the SCS (Figure 12g–l). The model deficiency adversely affects CanCM4's forecast for precipitation over the Korea-Japan region, Southern China and the SCS because of the large FE and small PE.

6 | SUMMARY AND DISCUSSION

In this study, the capabilities of three models in the NMME (CFSv2, CanCM3 and CanCM4) and their ensemble mean in forecasting the EASM were comprehensively evaluated

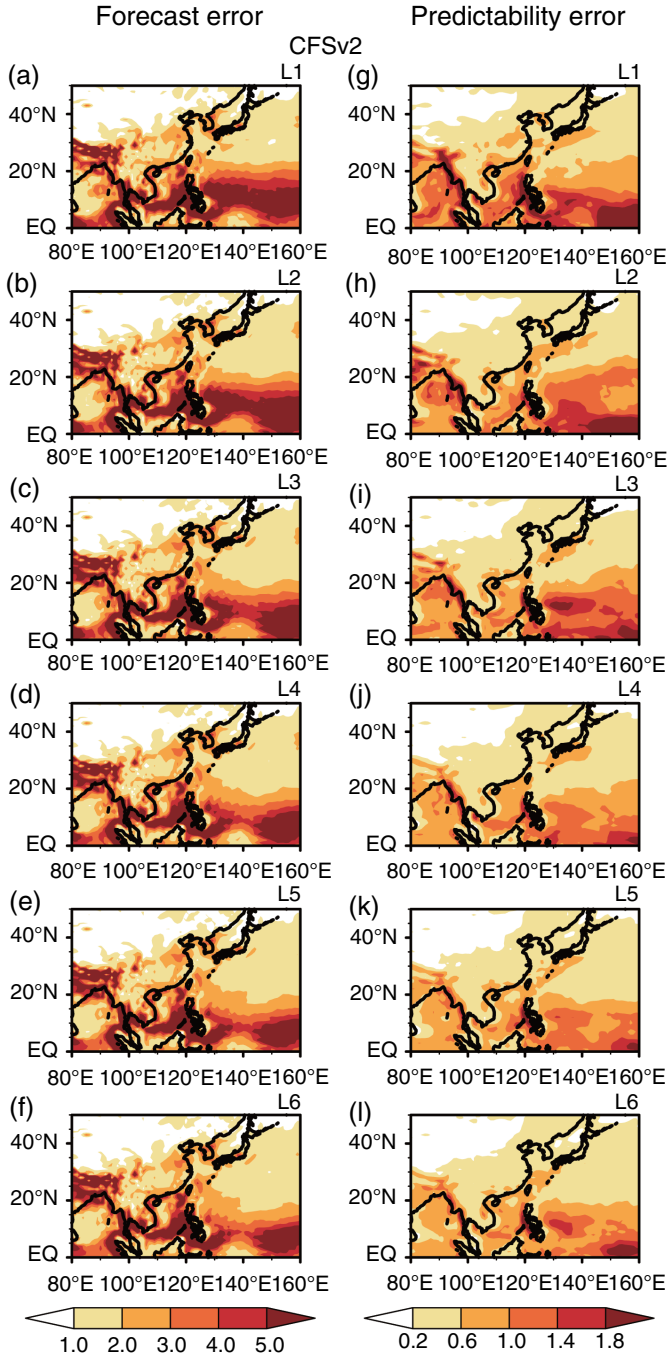

FIGURE 10 Forecast error (left) and predictability error (right) of the EASM precipitation for the CFSv2 hindcast at leads from 1 to 6 months

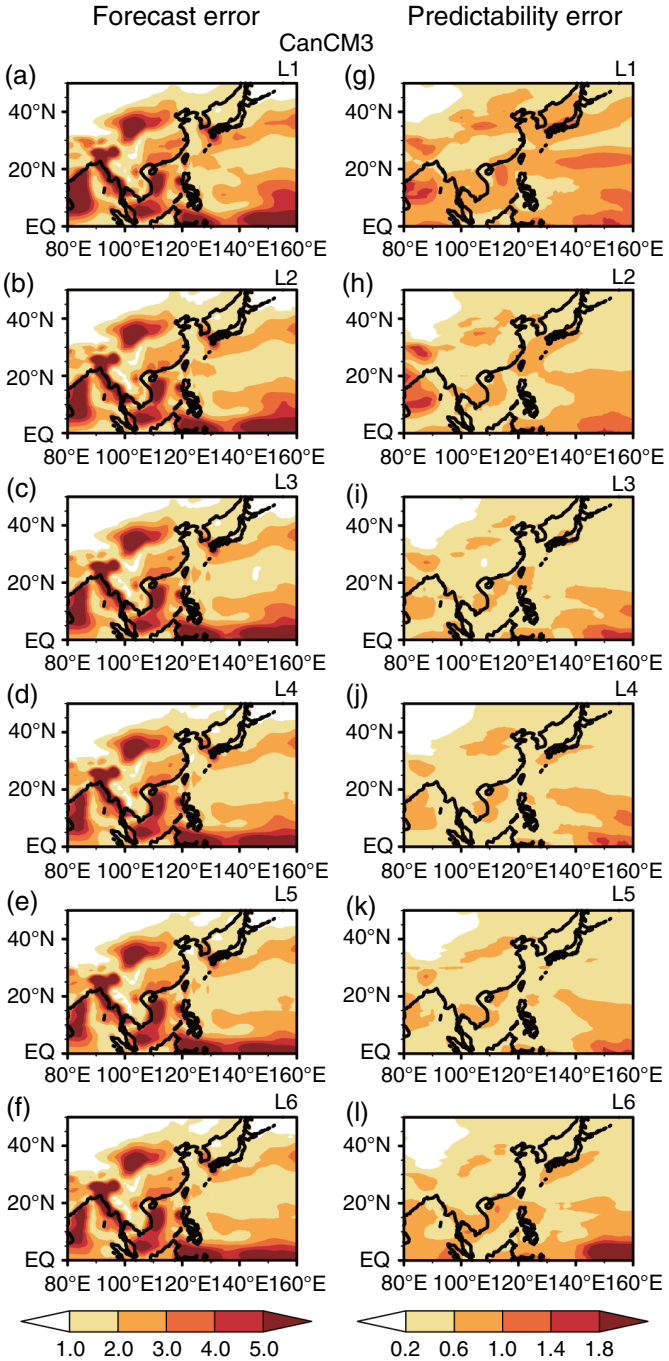

FIGURE 11 As in Figure 10 but for CanCM3

using hindcast data covering a 29-year period from 1982–2010. Their forecasts for EASM circulation and precipitation were examined in terms of the climatology and year-to-year variation. We also assessed the variation of forecast skill for the EASM indices as the leads increase and analysed the possible reasons limiting the forecast skill for the EASM. In addition, the sources of forecast error for EASM precipitation were studied through analysing the forecast error and predictability error. The key findings are summarized as follows.

The individual models can generally reproduce the climatological spatial distribution of the EASM circulation and precipitation. CFSv2 exhibits an abnormally weak monsoon trough over the SCS and a weak WNPSH. It also overestimates the precipitation over western China, the SCS and the WNP and underestimates the precipitation around eastern and Southern China as well as Korea. CanCM3 shows a northward-shifted WNPSH, corresponding to the strong dry

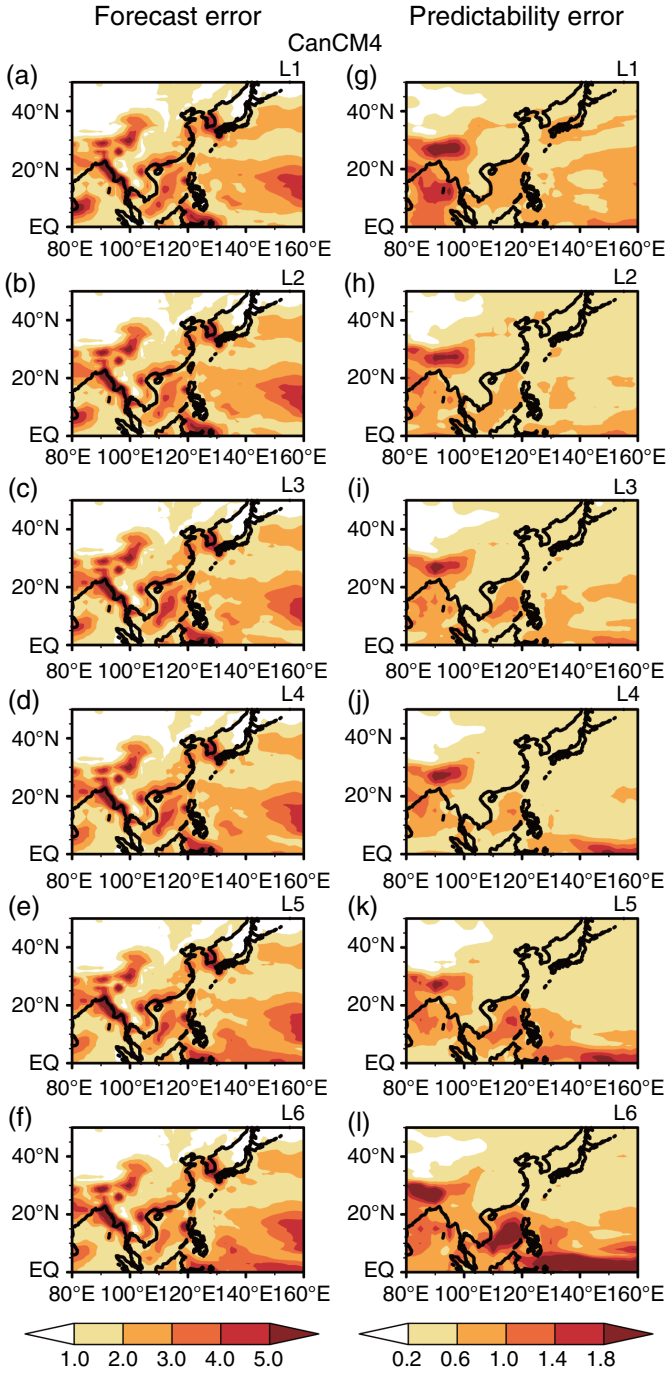

FIGURE 12 As in Figure 10 but for CanCM4

bias over the WNP and strong wet (dry) bias over central (southeast) China. CanCM4 generally exhibits the same bias pattern as CanCM3 but with a smaller bias, especially the precipitation bias over central China. Their MME obviously reduces the bias when forecasting the climatological features of EASM circulation and precipitation. For the intraseasonal evolution of EASM rainfall, CFSv2 performs the best overall, although the Meiyu-Changma-Baiu rainfall belt is slightly underestimated and the WNPSM rainfall belt is slightly southward-displaced. CanCM3 and CanCM4 have lower skill, with earlier monsoon onset and retreat than observations.

In addition to climatological features, the year-to-year variation of the EASM was evaluated. Two summer monsoon indices, that is, WNPSMI and EASMI, were considered. The forecast skill for the WNPSMI is generally higher than that for EASMI. The highest forecast skill, measured by the TCC, reached 0.84 for WNPSMI with the MME and 0.62 for the EASMI with CFSv2 at 0-month lead. The forecast skill generally decreases as the leads increase. Individual models show satisfactory forecasts for the WNPSMI at a 6-month lead. For the EASMI, only CFSv2 gives acceptable forecasts at leads up to 6 months, and the forecast skill of CanCM3 (CanCM4) decreases rapidly when the lead extends to 2 months (3 months). The failing forecasts for the EASMI from CanCM3 when the lead exceeds 2 months may be attributed to its weakness in capturing the relationship of the EASMI with the ENSO and NIOWNP SSTA. CanCM3's forecasts initiated in the preceding December, January, February and March fail to capture the positive relationship of the EASMI with the ENSO from the preceding winter to April or the positive relationship with the NIOWNP SSTA from May to July.

Finally, the sources of forecast error for EASM precipitation were analysed. Model error rather than the initial condition error is the main source of precipitation forecast error. However, the PE cannot be neglected from the 0-month lead to 2-month lead over the tropical western Pacific in CFSv2, over the WNP in CanCM3 and over the Tibetan Plateau in CanCM4.

As a fully coupled dynamical prediction system, CFSv2 has improved forecast skill compared to CFSv1 in forecasting the large-scale Asian summer monsoon circulation and precipitation patterns (Jiang *et al.*, 2013). In this study, CFSv2 shows useful skill for EASM variability and generally performs better than CanCM3 and CanCM4. CFSv2 has been evaluated in many studies but their focus was mainly on the Asian summer monsoon and Indian summer monsoon (Kim *et al.*, 2012; Shin and Huang, 2015; Pokhrel *et al.*, 2016; Ramu *et al.*, 2016; Rui *et al.*, 2016). In this study, we primarily focus on East Asia and comprehensively assess the EASM precipitation and circulations. The better performance of CanCM4 in forecasting the relationship of the EASMI with SST compared to CanCM3 shows the improvement of using a new generation of atmospheric general circulation models. The possible causes of the low skill for forecasting the EASMI with the CanCM4 long-lead forecasts are worth evaluating in the future, and the forecast skill for the EASM should also be evaluated. In addition, due to the unavailability of hindcast data from other NMME models, we evaluated only three models in this study. As

more hindcast data become available, other participating models should be included in the MME.

ACKNOWLEDGEMENTS

We would like to thank the reviewers for their helpful comments. We also thank Dr. Hai Lin at the Canadian Centre for Climate Modelling and Analysis for providing the CanCM3/CanCM4 hindcast data. This study is jointly supported by the National Programme on Global Change and Air–Sea Interaction (GASI-IPOVAI-03) and the NSFC Project (41305053).

ORCID

Huiwen Nie https://orcid.org/0000-0003-4939-4269
Yan Guo https://orcid.org/0000-0001-8169-2093

REFERENCES

Adler, R.F., Sapiano, M., Huffman, G.J., Wang, J., Gu, G., Bolvin, D., Chiu, L., Schneider, U., Becker, A., Nelkin, E., Xie, P., Ferraro, R. and Shin, D.B. (2018) The global precipitation climatology project (GPCP) monthly analysis (new version 2.3) and a review of 2017 global precipitation. *Atmosphere (Basel)*, 9(4), 14. https://doi.org/10.3390/atmos9040138.

Berrisford, P., Dee, D.P., Fielding, K., Fuentes, M., Kållberg, P.W., Kobayashi, S. and Uppala, S.M. (2009) The ERA-interim archive. *Era Report.*

Charney, J. and Shukla, J. (1981) Predictability of monsoons. In: J. Lighthill and RP Pearce, editors, *Monsoon Dynamics*. Cambridge, UK: Cambridge University Press.

Cherchi, A. and Navarra, A. (2002) Reproducibility and predictability of the Asian summer monsoon in the ECHAM4-GCM. *Climate Dynamics*, 20(4), 365–379. https://doi.org/10.1007/s00382-002-0280-6.

Ding, Y. (1991) Monsoons over China. *Atmospheric Science Library*, 419(2), 252–252.

Ding, Y. and Chan, J.C.L. (2005) The east Asian summer monsoon: an overview. *Meteorology & Atmospheric Physics*, 89(1–4), 117–142.

Du, Y., Xie, S.-P., Huang, G. and Hu, K. (2009) Role of air–sea interaction in the long persistence of El Niño–induced North Indian Ocean warming*. *Journal of Climate*, 22(8), 2023–2038. https://doi.org/10.1175/2008jcli2590.1.

Huang. (2014) An index measuring the interannual variation of the east Asian summer monsoon—the EAP index. *Advances in Atmospheric Sciences*, 21(1), 41–52. https://doi.org/10.1007/bf02915679.

Huang, B., Banzon, V.F., Freeman, E., Lawrimore, J., Liu, W., Peterson, T.C., Smith, T.M., Thorne, P.W., Woodruff, S.D. and Zhang, H.-M. (2015) Extended Reconstructed Sea surface temperature version 4 (ERSST.v4). Part I: upgrades and Intercomparisons. *Journal of Climate*, 28(3), 911–930. https://doi.org/10.1175/jcli-d-14-00006.1.

Huang, R., Zhang, Z., Huang, G. and Ren, B. (1998) Characteristics of water vapor transport in East Asian monsoon region and its differences from that of South Asian monsoon region in summer. *Scientia Atmospherica Sinica*, 22(4), 460–469. https://doi.org/10.3878/j.issn.1006-9895.1998.04.08 (in Chinese).

Huang, R. and Zhou, L. (2002) Research on the characteristics, formation mechanism and prediction of severe climate disasters in China. *Natural Disasters*, 11(1), 1–9. https://doi.org/10.3969/j.issn.1004-4574.2002.01.001 (in Chinese).

Jiang, X., Yang, S., Li, Y., Kumar, A., Liu, X., Zuo, Z. and Jha, B. (2013) Seasonal-to-interannual prediction of the Asian summer monsoon in the NCEP climate forecast system version 2. *Journal of Climate*, 26(11), 3708–3727. https://doi.org/10.1175/jcli-d-12-00437.1.

Kim, H.-M., Webster, P.J., Curry, J.A. and Toma, V.E. (2012) Asian summer monsoon prediction in ECMWF system 4 and NCEP CFSv2 retrospective seasonal forecasts. *Climate Dynamics*, 39(12), 2975–2991. https://doi.org/10.1007/s00382-012-1470-5.

Kirtman, B.P., Min, D., Infanti, J.M., Kinter, J.L., Paolino, D.A., Zhang, Q., van den Dool, H., Saha, S., Mendez, M.P., Becker, E., Peng, P., Tripp, P., Huang, J., DeWitt, D.G., Tippett, M.K., Barnston, A.G., Li, S., Rosati, A., Schubert, S.D., Rienecker, M., Suarez, M., Li, Z.E., Marshak, J., Lim, Y.-K., Tribbia, J., Pegion, K., Merryfield, W.J., Denis, B. and Wood, E.F. (2014) The north American multimodel ensemble: phase-1 seasonal-to-interannual prediction; phase-2 toward developing intraseasonal prediction. *Bulletin of the American Meteorological Society*, 95(4), 585–601. https://doi.org/10.1175/bams-d-12-00050.1.

Krishnamurti, T.N., Kishtawal, C., Zhang, Z., LaRow, T., Bachiochi, D., Williford, E., Gadgil, S. and Surendran, S. (2000) Multimodel ensemble forecasts for weather and seasonal climate. *Journal of Climate*, 13(23), 4196–4216.

Krishnamurti, T.N., Kishtawal, C.M., Larow, T.E., Bachiochi, D.R., Zhang, Z., Williford, C.E., Gadgil, S. and Surendran, S. (1999) Improved weather and seasonal climate forecasts from multimodel superensemble. *Science*, 285(5433), 1548–1550.

Lee Drbohlav, H.-K. and Krishnamurthy, V. (2010) Spatial structure, forecast errors, and predictability of the south Asian monsoon in CFS monthly retrospective forecasts. *Journal of Climate*, 23(18), 4750–4769. https://doi.org/10.1175/2010jcli2356.1.

Lee, S.-S., Lee, J.-Y., Ha, K.-J., Wang, B. and Schemm, J.K.E. (2011) Deficiencies and possibilities for long-lead coupled climate prediction of the Western North Pacific-East Asian summer monsoon. *Climate Dynamics*, 36(5–6), 1173–1188. https://doi.org/10.1007/s00382-010-0832-0.

Li, C., Lu, R. and Dong, B. (2012) Predictability of the western North Pacific summer climate demonstrated by the coupled models of ENSEMBLES. *Climate Dynamics*, 39(1–2), 329–346. https://doi.org/10.1007/s00382-011-1274-z.

Li, C., Scaife, A.A., Lu, R., Arribas, A., Brookshaw, A., Comer, R.E., Li, J., MacLachlan, C. and Wu, P. (2016) Skillful seasonal prediction of Yangtze river valley summer rainfall. *Environmental Research Letters*, 11(9), 094002. https://doi.org/10.1088/1748-9326/11/9/094002.

MacLachlan, C., Arribas, A., Peterson, K.A., Maidens, A., Fereday, D., Scaife, A.A., Gordon, M., Vellinga, M., Williams, A., Comer, R.E., Camp, J., Xavier, P. and Madec, G. (2015) Global seasonal forecast system version 5 (GloSea5): a high-resolution seasonal forecast system. *Quarterly Journal of the Royal Meteorological Society*, 141(689), 1072–1084. https://doi.org/10.1002/qj.2396.

Merryfield, W.J., Lee, W.-S., Boer, G.J., Kharin, V.V., Scinocca, J.F., Flato, G.M., Ajayamohan, R.S., Fyfe, J.C., Tang, Y. and

Polavarapu, S. (2013) The Canadian seasonal to interannual prediction system. Part I: models and initialization. *Monthly Weather Review*, 141(8), 2910–2945. https://doi.org/10.1175/mwr-d-12-00216.1.

Molteni, F., Stockdale, T., Balmaseda, M., Balsamo, G., Buizza, R., Ferranti, L., Magnusson, L., Mogensen, K., Palmer, T. and Vitart, F. (2011) *The New ECMWF Seasonal Forecast System (System 4)*. ECMWF Technical Memorandum 656.

Park, H.-J., Kryjov, V.N. and Joong-Bae, A. (2018) One-month lead predictability of Asian summer monsoon indices based on the zonal winds by APCC multi-model ensemble. *Journal of Climate*, 31, 8945–8960.

Pokhrel, S., Saha, S. K., Dhakate, A., Rahman, H., Chaudhari, H. S., Salunke, K., Hazra, A., Sujith, K., and Sikka, D. R. J. C. D. (2016). Seasonal prediction of Indian summer monsoon rainfall in NCEP CFSv2: forecast and predictability error. 46(7), 2305–2326. doi: https://doi.org/10.1007/s00382-015-2703-1

Ramu, D.A., Sabeerali, C.T., Chattopadhyay, R., Rao, D.N., George, G., Dhakate, A.R., Salunke, K., Srivastava, A. and Rao, S. A. (2016) Indian summer monsoon rainfall simulation and prediction skill in the CFSv2 coupled model: impact of atmospheric horizontal resolution. *Journal of Geophysical Research Atmospheres*, 121(5), 2205–2221.

Rui, C., Antúnez, O., Bebianno, M.J., Cajaraville, M.P. and Torreblanca, A. (2016) Large-scale teleconnection patterns of Indian summer monsoon as revealed by CFSv2 retrospective seasonal forecastruns. *International Journal of Climatology*, 36(9), 3297–3313.

Saha, S., Moorthi, S., Wu, X., Wang, J., Nadiga, S., Tripp, P., Behringer, D., Hou, Y.-T., Chuang, H.-y., Iredell, M., Ek, M., Meng, J., Yang, R., Mendez, M.P., van den Dool, H., Zhang, Q., Wang, W., Chen, M. and Becker, E. (2014) The NCEP climate forecast system version 2. *Journal of Climate*, 27(6), 2185–2208. https://doi.org/10.1175/jcli-d-12-00823.1.

Saha, S. K., Sujith, K., Pokhrel, S., Chaudhari, H. S., and Hazra, A. J. C. D. (2016). Predictability of global monsoon rainfall in NCEP CFSv2. 47(5), 1693–1715. doi:https://doi.org/10.1007/s00382-015-2928-z

Shi, L., Hendon, H.H., Alves, O., Luo, J.-J., Balmaseda, M.A. and Anderson, D.L.T. (2011) How predictable is the Indian Ocean dipole? *Monthly Weather Review*, 140(12), 3867–3884.

Shin, C.-S. and Huang, B. (2015) Slow and fast annual cycles of the Asian summer monsoon in the NCEP CFSv2. *Climate Dynamics*, 47(1–2), 529–553. https://doi.org/10.1007/s00382-015-2854-0.

Sooraj, K.P., Terray, P. and Mujumdar, M. (2014) Global warming and the weakening of the Asian summer monsoon circulation: assessments from the CMIP5 models. *Climate Dynamics*, 45(1–2), 233–252. https://doi.org/10.1007/s00382-014-2257-7.

Wan, R. and Wu, G. (2007) Mechanism of the spring persistent rains over southeastern China. *Science in China Series D: Earth Sciences*, 50(1), 130–144. https://doi.org/10.1007/s11430-007-2069-2.

Wang, B. and LinHo. (2002) Rainy seasons of the Asian-Pacific monsoon. *Journal of Climate*, 15(4), 386–398.

Wang, B. and Fan, Z. (1999) Choice of south Asian summer monsoon indices. *Bulletin of the American Meteorological Society*, 80(4), 629–638.

Wang, B., Wu, R. and Fu, X. (2000) Pacific–East Asian teleconnection: how does ENSO affect east Asian climate? *Journal of Climate*, 13(9), 1517–1536.

Wang, B., Wu, R. and Lau, K.M. (2001) Interannual variability of the Asian summer monsoon: contrasts between the Indian and the Western North Pacific-east Asian monsoons. *Journal of Climate*, 14(20), 4073–4090.

Wang, B., Zhang, Y. and Lu, M.M. (2004) Definition of South China sea monsoon onset and commencement of the East Asia summer monsoon. *Journal of Climate*, 17(4), 699–710.

Wu, R. and Wang, B. (2000) Interannual variability of summer monsoon onset over the Western North Pacific and the underlying processes. *Journal of Climate*, 13(14), 2483–2501.

Wu, Z., Wang, B., Li, J. and Jin, F.-F. (2009) An empirical seasonal prediction model of the east Asian summer monsoon using ENSO and NAO. *Journal Of Geophysical Research-Atmospheres*, 114 (D18), 13. https://doi.org/10.1029/2009jd011733.

Xie, S.-P., Kosaka, Y., Du, Y., Hu, K., Chowdary, J.S. and Huang, G. (2016) Indo-western Pacific Ocean capacitor and coherent climate anomalies in post-ENSO summer: a review. *Advances in Atmospheric Sciences*, 33(4), 411–432. https://doi.org/10.1007/s00376-015-5192-6.

Yuan, X., Wood, E.F., Luo, L. and Pan, M. (2011) A first look at climate forecast system version 2 (CFSv2) for hydrological seasonal prediction. *Geophysical Research Letters*, 38(13), 584–610. https://doi.org/10.1029/2011GL047792.

Yuan, Y., Yang, H., Zhou, W. and Li, C. (2008) Influences of the Indian Ocean dipole on the Asian summer monsoon in the following year. *International Journal of Climatology*, 28(14), 1849–1859. https://doi.org/10.1002/joc.1678.

Zhang, R., Sumi, A. and Kimoto, M. (1996) Impact of El Nino on the East Asian Monsoon. *Journal of the Meteorological Society of Japan. Series II*, 74(1), 49–62. https://doi.org/10.2151/jmsj1965.74.1_49.

Zhao, G., Huang, G., Wu, R., Tao, W., Gong, H., Qu, X. and Hu, K. (2015) A new upper-level circulation index for the east Asian summer monsoon variability. *Journal of Climate*, 28(24), 9977–9996. https://doi.org/10.1175/jcli-d-15-0272.1.

Zheng, J., Li, J. and Feng, J. (2014) A dipole pattern in the Indian and Pacific oceans and its relationship with the East Asian summer monsoon. *Environmental Research Letters*, 9(7), 074006. https://doi.org/10.1088/1748-9326/9/7/074006.

Zuo, Z., Yang, S., Hu, Z.-Z., Zhang, R., Wang, W., Huang, B. and Wang, F. (2013) Predictable patterns and predictive skills of monsoon precipitation in Northern Hemisphere summer in NCEP CFSv2 reforecasts. *Climate Dynamics*, 40(11–12), 3071–3088. https://doi.org/10.1007/s00382-013-1772-2.

How to cite this article: Nie H, Guo Y. An evaluation of East Asian summer monsoon forecast with the North American Multimodel Ensemble hindcast data. *Int J Climatol*. 2019;39:4838–4852. https://doi.org/10.1002/joc.6112